

FROM PIXELS TO FACTORS: LEARNING INDEPENDENTLY CONTROLLABLE STATE VARIABLES FOR REINFORCEMENT LEARNING

Anonymous authors

Paper under double-blind review

ABSTRACT

Algorithms that exploit *factored* Markov decision processes are far more sample-efficient than factor-agnostic methods, yet they assume a factored representation is known *a priori*—a requirement that breaks down when the agent sees only high-dimensional observations. Conversely, deep reinforcement learning handles such inputs but cannot benefit from factored structure. We address this representation problem with Action-Controllable Factorization (ACF), a contrastive learning approach that uncovers *independently controllable* latent variables—state components each action can influence separately. ACF leverages sparsity: actions typically affect only a subset of variables, while the rest evolve under the environment’s dynamics, yielding informative data for contrastive training. ACF recovers the ground-truth controllable factors directly from pixel observations on three benchmarks with known factored structure—TAXI, FOURROOMS, and MINIGRID-DOORKEY—consistently outperforming baseline disentanglement algorithms.

1 INTRODUCTION

Over the last decade, deep reinforcement learning (RL) has enabled agents to learn complex behaviors directly from high-dimensional observations—e.g., pixels in Atari games (Mnih et al., 2015), and continuous control from pixels (Lillicrap et al., 2016; Levine et al., 2016)—without manual feature engineering. However, this flexibility comes at a cost: modern deep RL methods remain strikingly sample-inefficient.

Classical work in factored RL shows that, if the underlying Markov decision process (MDP) can be decomposed into state-variable factors with sparse dependencies, one can achieve exponential gains in both model learning and planning (Boutillier et al., 1995; Guestrin et al., 2003). Indeed, factored variants of PAC-RL algorithms such as factored E^3 (Kearns & Koller, 1999) and Factored RMax (Guestrin et al., 2002; Brafman & Tennenholtz, 2002), provably exploit these structures for faster convergence, and subsequent methods even learn the dependency graph online (Strehl et al., 2007; Diuk et al., 2009). More recently, factored representations have proven useful for world modeling (Wang et al., 2022b; Pitis et al., 2020; 2022), exploration (Wang et al., 2023; Seitzer et al., 2021), and skill discovery (Vigorito & Barto, 2010; Wang et al., 2024; Chuck et al., 2024; 2025). Crucially, all these gains depend on having access to a hand-specified factored representation.

State-of-the-art model-based deep RL approaches avoid simulating trajectories in raw observations by learning latent world models end-to-end (Hafner et al., 2019; Schrittwieser et al., 2020; Hansen et al., 2022; Rodriguez-Sanchez & Konidaris, 2024). Some efforts attempt to induce factorization in these latent spaces (Hansen et al., 2022; Hafner et al., 2025), but they do not offer empirical or theoretical guarantee that any factor is identified. In parallel, unsupervised and self-supervised learning has long studied disentanglement (Bengio et al., 2013; Locatello et al., 2019) as a way to achieve better generalization. Although there is no consensus formalization of disentanglement, two classical approaches are nonlinear ICA (Independent Component Analysis; Comon (1994); Hyvärinen et al. (2023)) and causal representation learning (Schölkopf et al., 2021) yet these methods do not fully ground to decision making and control. For instance, some methods pretrain disentangled representations for RL (Higgins et al., 2017a) based on the assumption that the learned variables will

054 be useful for downstream decision-making. Meanwhile, causal representation learning (Schölkopf
055 et al., 2021) leverages the notion of interventions, related to an RL agent actions, but do not directly
056 address the sequential decision making problem.

057 We address this representation gap for factored RL by explicitly targeting the recovery of indepen-
058 dently controllable variables (Thomas et al., 2018). Our key idea is to use a contrastive objective that
059 compares the predicted next-state distributions under agent actions against those under the environ-
060 ment’s natural dynamics. Thus, we align our latent factors with the underlying state variables that
061 are controlled independently. We validate our approach on pixel-based versions of Taxi (Dietterich,
062 2000), MiniGrid-DoorKey (Chevalier-Boisvert et al., 2023; Pignatelli et al., 2024), and FourRooms
063 (Sutton et al., 1999), showing that we can automatically recover controllable state variables that align
064 with an expert-designed representation, directly from the pixels.

065 **Contributions** First, we formalize the representation learning problem for factored RL as the problem
066 of identifying *independently controllable* latent variables. Moreover, we propose a novel contrastive
067 learning objective that leverages action-induced discrepancies in next-state predictions to isolate
068 controllable factors. Finally, we demonstrate empirically that our method recovers ground-truth
069 controllable factors directly from pixels in classical RL domains.

071 2 BACKGROUND

072
073 **Markov Decision Process** We consider an agent that acts in a Markov Decision Process (MDP;
074 Puterman (1994)) $\mathcal{M} = \langle \mathcal{S}, A, T, R, p_0, \gamma \rangle$ with a continuous state space $\mathcal{S} \subseteq \mathbb{R}^{d_s}$ and a discrete
075 action set A . The transition function $T : \mathcal{S} \times A \rightarrow \Delta(\mathcal{S})^1$ models the world’s dynamics, $R : \mathcal{S} \times A \rightarrow$
076 \mathbb{R} is a reward function, $\gamma \in [0, 1)$ is the discount factor, and $p_0 \in \Delta(\mathcal{S})$ is the initial state distribution.

077 **Factored MDPs** (FMDPs; Boutilier & Dearden (1996)) are a particular class of MDPs that have a
078 factorized transition function:

$$080 T(s' | s, a) = \prod_{i=1}^K T_i(s'_i | \text{pa}(s'_i), a),$$

081 where the state space is $\mathcal{S} = \mathcal{S}_1 \times \dots \times \mathcal{S}_K$ and each $\mathcal{S}_i \subseteq \mathbb{R}$. Moreover, $\text{pa}(s'_i) : \mathcal{S}_i \rightarrow \mathcal{P}([K])$,
082 where $\mathcal{P}([K])$ is the power set of $[1, 2, \dots, K]$, and it represents the set of factors required to predict
083 s'_i . Typically, this structure is represented by a Dynamic Bayesian Network (DBN; Boutilier et al.
084 (1995; 2000)).

085
086 **Nonlinear Independent Component Analysis** (ICA; Comon (1994)) is the problem of identifying a
087 set of independent signal sources from entangled measurements. Formally, given a set of generating
088 sources $\{s_i \in \mathcal{S}_i\}_{i=1}^K$ that are independent and distributed according to densities $p(s_i)$, ICA identifies
089 the set of generating signals from observed measurements x that are entangled (mixed) by an unknown
090 function o —i.e., $x = o(s_1, \dots, s_K)$. In the case of non-linear ICA, o is a nonlinear, invertible
091 function. In particular, we will consider the problem of non-linear ICA with auxiliary variables
092 (Hyvärinen et al., 2019), where the sources to be identified are *conditionally* independent given an
093 auxiliary variable u . Moreover, we assume that our agent receives high-dimensional observations
094 that are generated by an observation function that is a diffeomorphism² $o : \mathcal{S} \rightarrow X \subseteq \mathbb{R}^{d_x}$, where
095 $d_x \gg d_s$.

097 3 ACF: ACTION CONTROLLABLE FACTORIZATION

098
099 Imagine a simple desk lamp with two separate switches: one toggles the lamp’s power, flipping
100 it on or off, while the other cycles the bulb’s color between warm and cold light. If you leave
101 both switches untouched, the lamp may still occasionally flicker on or change color on its own, but
102 with a significantly lower probability. By observing the lamp when you flip only the power switch
103 versus doing nothing, you isolate the “on/off” factor; likewise, by pressing only the color switch
104 versus leaving it alone, you isolate the “color” factor. Because each switch only affects one property
105 while the other property evolves naturally, you can disentangle these two characteristics simply by
106

107 ¹ $\Delta(X)$ is the set of probability densities over set X .

²A bijection that is continuously differentiable and whose inverse is also continuously differentiable.

108 contrasting action-driven changes with natural behavior. The lamp might have other characteristics
 109 like volume, weight, and shape; however, these are not factors that can be controlled by the agent.
 110 Here we focus on disentangling factors that *are* controllable.

112 3.1 PROBLEM FORMULATION

113
 114 **Setting** We consider that the agent does not have access to the ground truth factored state space S .
 115 Instead, it gets high-dimensional observations that are generated by an unknown diffeomorphism
 116 $o : \mathcal{S} \rightarrow X \subseteq \mathbb{R}^{d_x}$. Hence, we are concerned with learning from the observed samples of $T(x' | x, a)$
 117 an encoder $f_\phi : X \rightarrow Z$, where Z factorizes as $Z = Z_1 \times \dots \times Z_K$, that *identifies* the underlying
 118 factors.

119 **Identification** Formally, we say that a learned factorization identifies the underlying factor \mathcal{S}_i if and
 120 only if there exist invertible functions h_i and permutation function ρ such that $h_i : Z_i \rightarrow \mathcal{S}_{\rho(i)}$ for
 121 all $i \in \{1, \dots, K\}$. That is, we can recover the underlying factors up to permutation and invertible
 122 transformations.

123 In many problems, the agent’s actions have sparse effects on the environment: just a few factors are
 124 controlled, while others just follow their natural transition, unaffected by the agent. To help the agent
 125 understand its environment, we assume that the agent has a *special action* a_0 that corresponds to a
 126 *no-op* (or observe) action that allows the agent to observe the natural evolution of the environment
 127 without intervening.

128 **Transition Dynamics** Let $\Psi : \mathcal{S} \times A \rightarrow \mathcal{P}([1, 2, \dots, K])$ be the set of variables affected by action a
 129 in state s . We assume the transition dynamics factorize as follows,

$$131 T(s' | s, a) = \prod_{i \in \Psi(s, a)} T(s'_i | s, a) \prod_{j \notin \Psi(s, a)} T(s'_j | s, a_0); \quad (1)$$

132 where $T(s'_i | s, a_0)$ represents the natural (or observational) dynamics. In here, we will consider
 133 conditioning the transition dynamics on the full current state s , instead of just the parents, given that
 134 $T(s'_i | s, a) = T(s'_i | \text{pa}(s'_i), a)$.

135 Moreover, for the unknown observation function o , a diffeomorphism, we know that the *observed*
 136 dynamics follow (Boothby, 2003):

$$137 T(x' | x, a) = |\det (J_{o^{-1}}(x')^T J_{o^{-1}}(x'))|^{1/2} T(s' | s, a), \quad (2)$$

138 This equation relates the observed dynamics $T(x' | x, a)$ to the underlying ground truth state
 139 dynamics $T(s' | s, a)$ by the Jacobian matrix $J_{o^{-1}}$, whose determinant quantifies the change in
 140 volume between the two spaces. This relation can be seen as the generalization to higher dimensions
 141 of the change of variable formula in probability theory.

142 3.2 ALGORITHM

143 **Energy Parameterization** We parameterize the encoder by $f_\phi(x) \mapsto z$, with parameters ϕ , and, more
 144 importantly, we parameterize the transition function as the sum of energy functions (unnormalized
 145 probability densities) such that, $T(z' | z, a) \propto \exp\left(\sum_{i=1}^K E_\theta(z'_i, a, z)\right)$ with $i \in [K]$ and parameters
 146 θ . This sum of energies reflects the factorized structure where each energy represent the transition
 147 dynamics of latent variable z_i .

148 **Learning a Markov Representation** In order to estimate these energy functions from data and learn
 149 a Markov representation suitable for RL (Allen et al., 2021), we optimize the following training
 150 objectives. Firstly, we estimate the inverse dynamics I^π using our energy functions, as follows,
 151

$$152 I^\pi(a | z, z') = \frac{T(z' | z, a) \pi(a | z)}{\sum_{a'} T(z' | z, a') \pi(a' | z)} \propto \frac{\exp(\sum_i E_\theta(z'_i, a, z)) \pi(a | z)}{\sum_{a' \in A} \exp(\sum_i E_\theta(z'_i, a', z)) \pi(a' | z)}; \quad (3)$$

153 and because our action set is discrete, we can use a softmax multiclass classifier to learn our inverse
 154 function by minimizing the cross entropy loss:

$$155 \mathcal{L}_{\text{inv}}(\phi, \theta) = -\log I^\pi(a | z, z'). \quad (4)$$

Secondly, we use InfoNCE (Oord et al., 2018) to maximize the mutual information between z and z' : we use a batch B of $N - 1$ negative samples and 1 positive sample, and minimize the following loss,

$$\mathcal{L}_{\text{fwd}}(\phi, \theta) = -\log \frac{\exp(\sum_i E_\theta(z'_i, a, z))}{\sum_{z^j \in B} \exp(\sum_i E_\theta(z'_i, a, z))}. \quad (5)$$

Optimizing these losses guarantee that we learn a Markov representation that preserves the relevant information for action effects prediction (Allen et al., 2021) without requiring an explicit reconstruction loss. However, they do not ensure that the representation will align with the controllable factors.

To see this, consider an invertible mapping $g : S \rightarrow Z$ between the ground truth state s and another representation z . The relation between the densities is given by the following change of variable formula: $T(s' | s, a) = |\det J_g(s')| T(z' | z, a)$. Therefore, if $|\det J_g(s')| = 1$ (e.g., g is a rotation), the distribution will match even in the case we use a factorized prior (for an extended discussion, see Locatello et al. (2019); Hyvärinen et al. (2023))

Factorizing the Controllable Variables We formalize our intuition and exploit the sparsity of the actions' effects to learn a latent representation Z that identifies the controllable factors.

The core idea is to contrast the effect of an action, the distribution $T(x' | x, a)$, against the natural dynamics $T(x' | x, a_0)$, where a_0 is the no-op action, using the following ratio:

$$\begin{aligned} \log r_a(x', x) &= \log \frac{T(x' | x, a)}{T(x' | x, a_0)} = \log \frac{|\det(J_{o^{-1}}(x')^T J_{o^{-1}}(x))|^{1/2} \prod_i T(s'_i | s, a)}{|\det(J_{o^{-1}}(x')^T J_{o^{-1}}(x))|^{1/2} \prod_i T(s'_i | s, a_0)}; \\ &= \log \frac{T(s'_j | s, a)}{T(s'_j | s, a_0)} = \log r_a(s', s), \end{aligned}$$

where s'_j is the factor affected by a when executed in s . Therefore, this ratio is a function of the factor s'_j and not the rest.

In practice, we can estimate these ratios from observed transitions contrastively (Gutmann & Hyvärinen, 2010; Hyvärinen et al., 2019). We leverage our energy parameterization to infer a binary classifier that differentiate between transitions from action a from another, e.g. the null action a_0 .

These classifiers can be computed from the energies using a sigmoid function σ :

$$\sigma(\log r_a(z', z)) := \sigma(\log r_a(f_\phi(x'), f_\phi(x))) = \sigma \left(\sum_i E_\theta(z'_i, a, z) - E_\theta(z'_i, a_0, z) \right).$$

Finally, we train our energy functions to match the observed ratios by training $|A| - 1$ classifiers computed by $\sigma(\log r_a(z', z))$. We use the transitions of other actions as negative samples and minimize the following binary cross-entropy loss:

$$\mathcal{L}_r(\theta, \phi) = \sum_{a' \in A} [a' = a] \log \sigma(\log r_a + \zeta_a) + [a' \neq a] \log(1 - \sigma(\log r_a + \zeta_a)); \quad (6)$$

where $[\cdot]$ is indicator functions that is 1 when the condition holds, and $\zeta_a := \log \frac{\pi(a|z)}{\pi(a_0|z)}$ are correction weights to account for the policy used to collect the data. In practice, we estimate the policy from the dataset and use the estimate to compute the loss. Finally, we minimize a weighted sum of these losses and use AdamW as our optimizer (Loshchilov & Hutter, 2019). Algorithm 1 formalizes the approach.

Identifiability The core assumption of ACF is that variables are independently controllable, that is, for every state variable s_i , there exists a context $s \in \mathcal{S}$ and action $a \in A$, where the action effect is sufficiently different from the natural dynamics of the variable (a_0 effect). The following theorem establishes identifiability of independently controllable factors if the solution found is sparse.

Theorem 3.1 (Identifiability of the Independently Controllable Factors). *Let the learned encoder $f : X \rightarrow Z$ be a diffeomorphism. If the following conditions hold*

Algorithm 1 Action Controllable Factorization

Require: Dataset $\mathcal{D} = \{(x, a, x')\}$, encoder f_ϕ , set per-factor energy models $\{E_\theta^k\}_{k=1}^K$, policy π_w , Learning rate α , weights $\beta_r, \beta_{\text{fwd}}, \beta_{\text{inv}}, \beta_\pi$

- 1: **for** minibatch $\{(x^n, a^n, x'^n)\}_{n=1}^N \sim \mathcal{D}$ **do**
- 2: Encode: $z^n \leftarrow f_\phi(x^n), z'^n \leftarrow f_\phi(x'^n)$
- 3: Noise: $z^n \leftarrow z^n + \varepsilon^n, z'^n \leftarrow z'^n + \varepsilon'^n$
- 4: Negatives: $\mathcal{N} = \{(z^i, a^j, z'^j) \mid i, j = 1, \dots, N\}$
- 5: Energies: $E_{ij}(a) = \sum_k E_\theta^k(z_k^j, a, z^i) \forall i, j \in [N], k \in [K], a \in A$
- 6: Policy logits: $\pi_{\text{logits}}^n = \pi_w(z^n) \forall n$
{The diagonal values are the energy that correspond to real transitions}
- 7: Ratios: $\log r_a^{nn} = E_{nn}(a) - E_{nn}(a_0)$
- 8: Policy weights: $\zeta_a^n = \log \frac{\pi(a_n | z^n)}{\pi(a_0 | z^n)}$
- 9: $\mathcal{L}_r = -\frac{1}{N} \sum_n \sum_a [a^n = a] \log \sigma(\log r_a^{nn} + \text{sg}(\zeta_a^n)) + [a^n \neq a] \log(1 - \sigma(\log r_a^{nn} + \text{sg}(\zeta_a^n)))$
- 10: $\mathcal{L}_{\text{fwd}} = -\frac{1}{N} \sum_n \log \frac{1}{\sum_j e^{E_{nj}(a^n)}}$
- 11: $\mathcal{L}_{\text{inv}} = -\frac{1}{N} \sum_n \log \frac{\pi(a^n | z^n) e^{E_{nn}(a^n)}}{\sum_{a'} \pi(a' | z^n) e^{E_{nn}(a')}}$
- 12: $\mathcal{L}_\pi = \frac{1}{N} \sum_n -\log \frac{e^{\pi_{\text{logits}}^n[a^n]}}{\sum_{a'} e^{\pi_{\text{logits}}^n[a']}}$
- 13: $\mathcal{L} = \beta_r \mathcal{L}_r + \beta_{\text{fwd}} \mathcal{L}_{\text{fwd}} + \beta_{\text{inv}} \mathcal{L}_{\text{inv}} + \beta_\pi \mathcal{L}_\pi$
- 14: Update: $(\phi, \theta, w) \leftarrow \text{AdamW}((\phi, \theta, w), \alpha, \nabla \mathcal{L})$
- 15: **end for**

1. $\mathcal{S} \subset \mathbb{R}^K$ is connected and the unknown observation function $o : \mathcal{S} \rightarrow X$ is a diffeomorphism.

2. The action effects are **sufficiently different** from the natural dynamics. That is, there exists $i \in [K]$

$$\frac{\partial T_i(s'_i | s, a)}{\partial s'_i T(s'_i | s, a_0)} \neq 0$$

for $s \in \tilde{\mathcal{S}} \subseteq \mathcal{S}$, almost surely. Moreover, there exists at least an action that affects each s_i (independent controllability)

3. All energy function approximate the factor forward dynamics $E(z'_i, a, z) \propto \log T(z'_i | z, a)$;

4. (**Sparsity**) The score differences (gradients of the energies)

$$\frac{\partial}{\partial z'_i} \Delta E_i^a = \frac{\partial}{\partial z'_i} [E(z'_i, a, z) - E(z'_i, a_0, z)] \neq 0$$

for at most one variable j and all actions.

then, there exists a factor-wise diffeomorphism $h : \mathcal{S} \rightarrow Z$ between the underlying ground truth factors of variation \mathcal{S} and the learned encoding Z

Similar arguments have been used to establish identifiability under action and state-dependency sparsity (Lachapelle et al., 2022; 2024) and under single-node interventions in causal representation learning (Varici et al., 2024). Theorem 3.2 can be viewed as a special case of these results adapted to the independently controllable factors setting³. This result further shows that independently controllable factors can be recovered when, in addition to certain regularity and variability conditions, the solution is sparse (Condition 4). We conjecture that the binary classifiers arising from the \mathcal{L}_r loss promote sparsity by *competing* to capture what makes each action distinct with respect to both the natural dynamics and the other actions—namely, the specific factor influenced by the action. In the

³The proof is provided in Appendix A

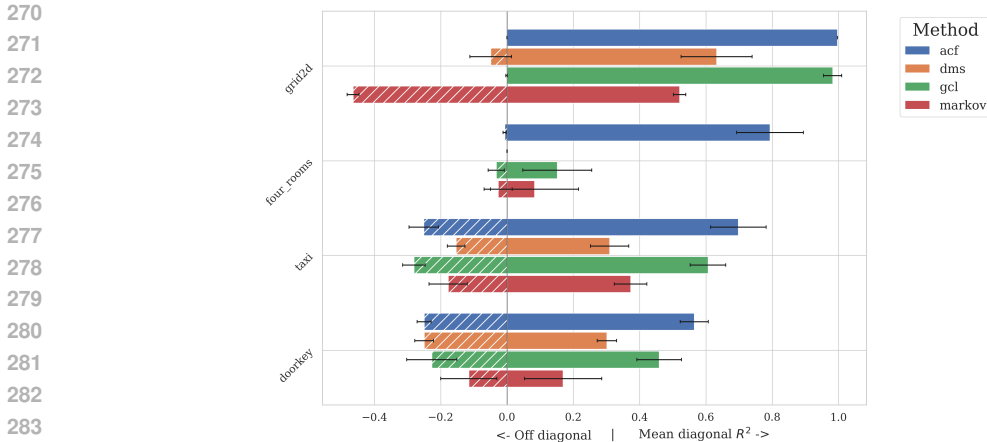


Figure 1: **Factorization metrics.** The left side bars show how much of the information is represented off the diagonal on average over all variables. The right side bars represent the mean diagonal value. Ideally, we would expect our R^2 matrices to be close to the identity: 0 on the left bar, 1 on the right bar. The error bars show the standard deviation over 5 independent seeds.

next section, we demonstrate empirically that ACF indeed identifies the independently controllable factors in practice.

4 EVALUATION

In this section, we empirically evaluate ACF in RL test domains directly from pixel observations. We consider the visual variation of the classical Taxi domain (Dietterich, 2000) and visual Minigrid environments (Chevalier-Boisvert et al., 2023): FourRooms (Sutton et al., 1999) and DoorKey⁴. We chose these domains because they allow easy access to the generating factors for evaluation and while these domains are simple from the perspective of learning a policy, they actually are challenging from the factorization problem perspective, as we will see in the quantitative results.

Baselines We consider GCL (Generalized Contrastive Learning; Hyvärinen et al. (2019)) that can be seen as a vanilla contrastive-based disentanglement algorithm, and DMS (Disentanglement via Mechanism Sparsity; Lachapelle et al. (2022)), a VAE-based (Kingma & Welling, 2014) method that explicitly maximizes sparsity in state dependencies and action effects to drive disentanglement. Moreover, we consider MSA (Markov State Abstractions; Allen et al. (2021)), a contrastive-based algorithm that leverages both forward and inverse dynamics to learn Markovian representations but does not explicitly optimize for disentanglement. **It is important to notice that previous work has theoretically shown that methods that lack the correct inductive biases will converge to entangled representations almost surely (Locatello et al., 2019), therefore, we do not include these as baselines for our identification evaluation.**

Evaluation Protocol To measure disentanglement, we consider test datasets of pairs of $\{(s^i, z^i)\}_i$ where s is the ground truth representation and z is the corresponding learned latent representation. Then, we fit factor-wise regressors (parameterized by feed-forward networks), $h_{ij}(z_i) \mapsto s_j$. The performance of h_{ij} is limited by the amount of information z_i contains about s_j , therefore we measure the quality of the learned regressor using the coefficient of determination R^2 . Therefore, for each method we have a matrix R^2 (see Figure 2); this matrix would have 1 in the diagonal and low off-diagonal values if the ground truth variables were perfectly identified. We tune all methods via random search in their respective hyperparameter space and train 5 seeds for each method (see Appendix B).

Quantitative results Given a R^2 matrix, we search a permutation that maximizes the diagonal using the Hungarian algorithm (Kuhn, 1955). We then aggregate the matrices into two scores, the mean diagonal value, $\frac{1}{K} \sum_i R^2_{ii}$ and the mean maximum off-diagonal value $\frac{1}{K} \sum_i \max_{j \neq i} R^2_{ij}$. The

⁴We use Minigrid JAX (Bradbury et al., 2018) re-implementation (Pignatelli et al., 2024)

324
325
326
327
328
329
330
331
332
333
334
335
336
337
338
339
340
341
342
343
344
345
346
347
348
349
350
351
352
353
354
355
356
357
358
359
360
361
362
363
364
365
366
367
368
369
370
371
372
373
374
375
376
377

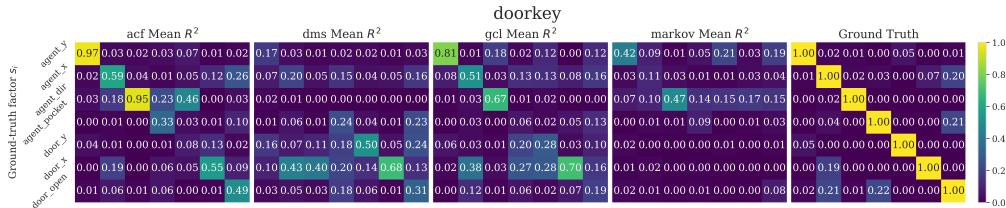


Figure 2: Factorization matrices for DoorKey. Mean R^2 matrices over 5 seeds.

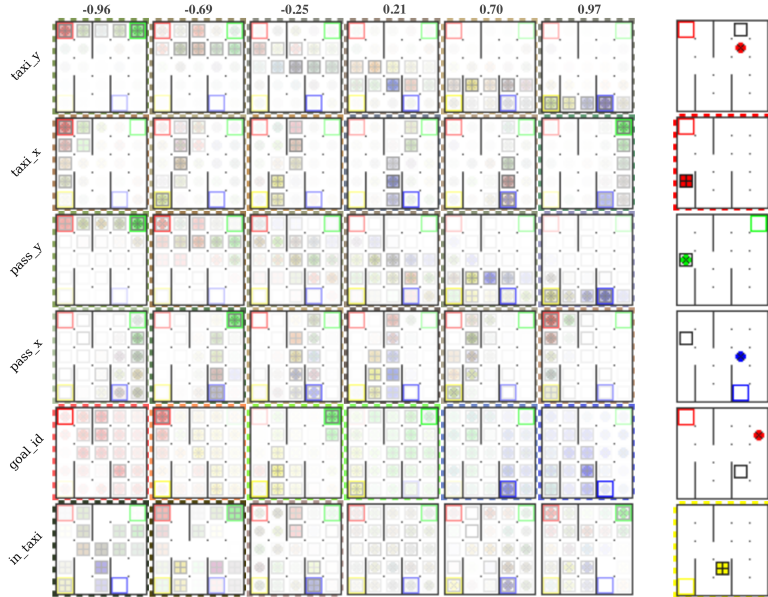


Figure 3: Taxi latent traversals. In this Taxi rendering, the taxi is represented by a hollow square, the passengers are circles with colors matching their goal positions. When a passenger is in the taxi, the border of the frame is highlighted with stripes. By varying the value of a latent variable (columns), we can see its effect on the mean observation. Each row represents different latent variables.

former measures how well a latent factor represents the ground truth factor, and the latter measures how much information is contained in the rest of the factors. Ideally, this would mean a score of 1 for the mean diagonal and 0 for the off diagonal if the identification is perfect and the factors are fully independent. However, this is only an upper bound on perfect performance in many environments; e.g. taxi and passenger’s position are not fully independent because the passenger can only move if it moves with the taxi. Figure 1 shows the results for all methods and domains.

The factor affected by an action depends on the current state s . Grid2D and FourRooms have different factorizations: In grid2D the agent can move up, down, left and right and 2 dimensions are enough as controllable factors, but in FourRooms (Minigrid variant) the agent can rotate, move forward, backward, left or right and, hence, 3 factors are required. More importantly, the factor an action affects is *relative to the agent’s orientation* and, this, change causes difficulties for all baseline methods. In particular, DMS, which assumes a global sparse graph, struggles to converge.

Factors are not independent In the Taxi domain, factorization is more challenging because the taxi’s position and the passenger’s location are inherently coupled; the passenger can move only if it moves with the taxi. Our method outperforms the baselines in this case. Figure 3 shows qualitatively the effect of traversing the identified passengers position variables.

Identifying non-controllable variables In the DoorKey domain, not all factors are controllable by the agent: the door’s position is sampled at the start of each episode and kept fixed throughout the episode. Although the agent must perceive the door’s location to open it, that factor need not be disentangled. In fact, as seen in Figure 2, the door y coordinate is not identified. DMS, instead is able

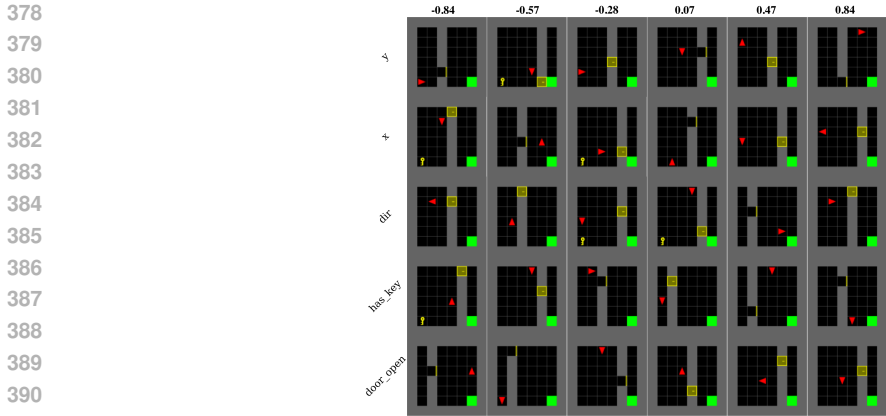


Figure 4: **DoorKey latent traversals.** For this domain, we show a random sample from observations that have a particular value of the latent dimension. We only show the controllable elements in DoorKey, that includes the agent position and orientation, the key and the door state. Different rows correspond to different latent variables and different columns represent different values for the corresponding latent variable.

to partially identify these variables because it’s not constrained to controllable elements and uses the sparsity of the state dependencies.

Ablation We performed an ablation study in the Minigrid-Doorkey domain, the most challenging environment considered in the previous experiments. Table 1 shows that each loss term plays an important role in improving factorization. In addition, we evaluate the *Factored Markov* variant, which combines our unified factored energy parameterization with the MSA losses (forward and inverse). This variant achieves improved factorization compared to the original MSA, highlighting the importance of the our proposed parameterization.

Experiment	Diag Score (Mean \pm Std) \uparrow	Off-Diag Score (Mean \pm Std) \downarrow
ACF (full)	0.5650 \pm 0.0423	0.2499 \pm 0.0213
Factored Markov	0.4861 \pm 0.0491	0.2635 \pm 0.0339
no fwd	0.1987 \pm 0.0588	0.1028 \pm 0.0340
no inv	0.5294 \pm 0.0274	0.1918 \pm 0.0280
no policy	0.4630 \pm 0.0694	0.2301 \pm 0.0543
no ratio	0.5083 \pm 0.0767	0.2353 \pm 0.0352

Table 1: Ablation on Minigrid-Doorkey Environment over 5 seeds

5 RELATED WORKS

Factored RL There is a long history of leveraging the structure of FMDPs for efficient planning algorithms. By assuming that the structure of the MDP is known (i.e., the DBN), these algorithms exponentially reduce the size of the problem representation. Such algorithms include Structured Value Iteration algorithms (Boutillier & Dearden, 1996; Boutillier et al., 2000) and Structured Policy Iteration (Boutillier et al., 1995; Koller & Parr, 2000), and their extensions to linear approximation (Guestrin et al., 2003). In classical PAC model-based RL algorithms, the Factored E^3 algorithm (Kearns & Koller, 1999) extends the E^3 algorithm (Kearns & Singh, 2002) to the case where the DBN is known and an oracle factored planner is available. Guestrin et al. instantiate this algorithm and RMax Brafman & Tennenholtz (2002) using factored linear value iteration (Guestrin et al., 2002) as the planner. Algorithms such as SLF-RMax (Strehl et al., 2007), Met-RMax (Diuk et al., 2009) and SPITI (Degris et al., 2006) loosen the assumption of a known DBN structure and discover this structure online for discrete state spaces. Vigorito & Barto (2009) extends structure learning to continuous state and action spaces. Further theoretical work includes regret bounds for factored RL

432 in the episodic (Osband & Van Roy, 2014; Tian et al., 2020) and non-episodic settings (Xu & Tewari,
433 2020).

434 The discovery of the structure among the factored state variables has been used to do exploration
435 (Seitzer et al., 2021; Wang et al., 2023). Closely related, in skill discovery, the factored structure can
436 be exploited to generate signals that facilitate learning useful skills (Vigorito & Barto, 2010; Hu et al.,
437 2024; Wang et al., 2024; Chuck et al., 2024; 2025). Moreover, leveraging the sparsity of edges in the
438 DBN enables algorithms to learn modular world models that are robust (Wang et al., 2022b; Ke et al.).
439 Counterfactual Data Augmentation (CODA) (Pitis et al., 2020; 2022) uses the *local* DBN structure to
440 generate plausible transitions by recombining states based on conditional independence relations that
441 hold locally—i.e., leverages local DBNs to have a nonparametric transition model. However, all of
442 these require knowing the factored representation a priori for these methods to work.

443 Limited attempts exist to learn factorized representations in deep RL from high-dimensional observa-
444 tions. DARLA (Higgins et al., 2017b) leverages β -VAE representations for zero-shot generalization
445 in multitask RL. Some works that try to learn factored world models include variational causal
446 dynamics models (Lei et al., 2022) and provable factored RL (Misra et al., 2021). DenoisedMDP
447 (Wang et al., 2022a; Liu et al., 2023) factorizes the state in four factors based on their relevance to
448 reward and controllability. TED (Temporal Disentanglement; Dunion et al. (2023)) uses NCE from
449 state transition samples to improve model-free agent robustness to correlated, irrelevant features,
450 and CMID (Conditional Mutual Information for Disentanglement; Dunion et al. (2024)) uses causal,
451 graphical conditions to infer the state factor from pixels. Perhaps, most similar to ours, is the work of
452 Thomas et al. (2018) that proposes to learn independently controllable elements by learning policies
453 that minimize the number of variables changed. However, they obtain limited success in fully aligning
454 a 2D grid learned representation with the ground truth.

455 **Controllability-based Representations for RL** There is an extensive literature that focuses on the
456 problem of reconstruction-free representations (Gelada et al., 2019; Zhang et al., 2021; Nguyen et al.,
457 2021; Lee et al., 2020) and abstractions for RL. Moving away from reconstruction objectives allows
458 more robust performance to temporally-correlated noise (Zhang et al., 2021; Wang et al., 2022a;
459 Rudolph et al., 2024; Ortiz et al., 2024). Importantly, and related to our approach, controllability has
460 been proven useful to learn deep representations that are sufficient for RL agents. Learning inverse
461 models (Lamb et al., 2023; Allen et al., 2021; Yi et al., 2023; Rudolph et al., 2024) has proven useful
462 to learn representations that capture the controllable components of the state. However, because
463 inverse models are insufficient (Lamb et al., 2023; Allen et al., 2021), they have been complemented
464 by multi-step inverse models (Lamb et al., 2023) and forward models (Allen et al., 2021). Factorizing
465 controllable variables has been explored in the past by DenoisedMDP (Wang et al., 2022a), they
466 assume known block factorization to separate variables across two axes (controllable/uncontrollable
467 and reward relevant/irrelevant). Follow up work propose an identifiable approach to the DenoisedMDP
468 idea (Liu et al., 2023). However, their approach does not encourage the disentanglement within the
469 blocks. ACF, though only focuses on the controllable variables, is designed to factorize to a finer
granularity.

470 **Disentanglement in Representation Learning** In representation learning (Bengio et al., 2013),
471 disentanglement has been extensively studied (Schmidhuber, 1992; Higgins et al., 2017a; Burgess
472 et al., 2018; Chen et al., 2018; Klindt et al., 2020) as a desirable characteristic for generalizable repre-
473 sentations. However, a widely accepted definition of disentanglement does not yet exist and solving
474 this problem without the right inductive biases is impossible (Locatello et al., 2019). Unsupervised
475 approaches leverage the Variational Autoencoder (VAE; Kingma & Welling (2014)) to learn latent
476 representations that have a factorized prior (Kim & Mnih, 2018), minimize total correlation (Chen
477 et al., 2018), and leverage temporal relations (Klindt et al., 2020). An important formalization of
478 disentanglement is Independent Component Analysis (ICA; Comon (1994)). In particular, non-linear
479 ICA (Hyvärinen et al., 2023), where a set of source variables is entangled by an unknown non-linear
480 function. Approaches in non-linear ICA include contrastive methods (Hyvärinen et al., 2019; Hyväri-
481 nen & Morioka, 2016), energy functions (Khemakhem et al., 2020b), quantized methods (Hsu et al.,
482 2024a;b), VAEs (Khemakhem et al., 2020a; Klindt et al., 2020) and sparse graphical conditions such
483 as DMS (Disentanglement via Mechanism Sparsity; Lachapelle et al. (2022)) Another approach is
484 causal representation learning (Schölkopf et al., 2021). This tackles the problem of discovering the
485 *causal* variables by leveraging data coming from interventional and observational distributions. In
this problem, the variables are not assumed to be independent as in ICA. Simple methods assume
having access about what variable was intervened (Lippe et al., 2022; 2023b; Locatello et al., 2020)

and assume binary interventions (Lippe et al., 2023a). Recent works establish identifiability results for linear mixing models (Squires et al., 2023), non-linear mixing (Ahuja et al., 2023; Buchholz et al., 2023; Zhang et al., 2023) and non-parametric in the case of unknown interventions (i.e., without labels of the intervened variable) (von Kügelgen et al., 2024; Varici et al., 2024). ACF can be interpreted as a special case where the agent’s actions induce interventional distributions and the natural dynamics are simply the observational distributions.

6 DISCUSSION AND LIMITATIONS

ACF takes a step toward closing the factored-representation gap: the longstanding challenge of identifying independently controllable latent variables directly from high-dimensional observations. Our focus in this work is not on demonstrating downstream RL gains—prior work has already shown that when a factored representation is available, RL can benefit substantially—but rather on the foundational question of whether such factors can be reliably recovered from pixels. A key strength of ACF is that it does not assume intervention masks (Lippe et al., 2022; 2023b; Locatello et al., 2020), one-to-one mappings between actions and state variables (Lippe et al., 2023a), nor determinism or static-world dynamics (Thomas et al., 2018). Instead, ACF leverages actions as soft interventions and allows the effect of an action to depend on context, improving over prior disentanglement and controllable-state approaches. The simplicity of our evaluation domains is intentional: these environments provide accessible ground-truth factors, allowing us to directly evaluate whether the learned latent space matches the factored structure.

At the same time, important limitations remain. ACF assumes that the immediate effect of an action can be observed; thus long-term, delayed action effects still pose a challenge. Similarly, while nothing in the formulation requires discrete actions, continuous-control environments often exhibit precisely such delayed effects, and handling them requires additional considerations that we left for future work, as they deserve their own separate treatment. Finally, ACF assumes that the controllable factors are present in the observations; partial observability, oclusions, and nuisance variation require additional assumptions that are orthogonal to the identifiability question we study here.

These limitations outline clear directions for future work: integrating temporally extended actions or skills, extending ACF to partial observability, and incorporating the method into world-model or model-based RL frameworks where identified controllable variables can directly contribute to improved generalization and sample efficiency.

7 CONCLUSION

We introduced a new contrastive algorithm for learning a factored representation that recovers the independently controllable variables from high-dimensional observations. We use the fact that RL agents can act upon their environments and create discrepancies in the dynamics; contrasting those controlled dynamics to the natural order of things provides a signal for disentanglement that is relevant for factored RL. Moreover, we showed empirically that our method is able to recover the relevant controllable factors.

ACF shows that agent intervention and control over its environment is an important direction to achieve disentanglement. The converse is also relevant, a drive to discover the world structure should be explored as a new intrinsic signal for agent exploration, learning and skill discovery: *the agent needs to actively learn complex behavior and experiment to discover the structure of its environment.*

REFERENCES

- Kartik Ahuja, Divyat Mahajan, Yixin Wang, and Yoshua Bengio. Interventional causal representation learning. In *International conference on machine learning*, pp. 372–407. PMLR, 2023.
- Cameron Allen, Neev Parikh, Omer Gottesman, and George Konidaris. Learning Markov state abstractions for deep reinforcement learning. *Advances in Neural Information Processing Systems*, 34:8229–8241, 2021.
- Yoshua Bengio, Aaron Courville, and Pascal Vincent. Representation learning: A review and new perspectives. *IEEE transactions on pattern analysis and machine intelligence*, 35(8):1798–1828, 2013.

- 540 William M Boothby. *An introduction to differentiable manifolds and Riemannian geometry, Revised*,
541 volume 120. Gulf Professional Publishing, 2003.
- 542
- 543 Craig Boutilier and Richard Dearden. Approximate value trees in structured dynamic programming.
544 In *Proceedings of the Thirteenth International Conference on International Conference on Machine*
545 *Learning*, pp. 54–62, 1996.
- 546 Craig Boutilier, Richard Dearden, Moisés Goldszmidt, et al. Exploiting structure in policy construc-
547 tion. In *IJCAI*, volume 14, pp. 1104–1113, 1995.
- 548
- 549 Craig Boutilier, Richard Dearden, and Moisés Goldszmidt. Stochastic dynamic programming with
550 factored representations. *Artificial intelligence*, 121(1-2):49–107, 2000.
- 551 James Bradbury, Roy Frostig, Peter Hawkins, Matthew James Johnson, Chris Leary, Dougal
552 Maclaurin, George Necula, Adam Paszke, Jake VanderPlas, Skye Wanderman-Milne, and
553 Qiao Zhang. JAX: composable transformations of Python+NumPy programs, 2018. URL
554 <http://github.com/jax-ml/jax>.
- 555
- 556 Ronen I Brafman and Moshe Tennenholtz. R-max-a general polynomial time algorithm for near-
557 optimal reinforcement learning. *Journal of Machine Learning Research*, 3(Oct):213–231, 2002.
- 558
- 559 Simon Buchholz, Goutham Rajendran, Elan Rosenfeld, Bryon Aragam, Bernhard Schölkopf, and
560 Pradeep Ravikumar. Learning linear causal representations from interventions under general
561 nonlinear mixing. *Advances in Neural Information Processing Systems*, 36:45419–45462, 2023.
- 562
- 563 Christopher P Burgess, Irina Higgins, Arka Pal, Loic Matthey, Nick Watters, Guillaume Des-
564 jardins, and Alexander Lerchner. Understanding disentangling in beta-VAE. *arXiv preprint*
565 *arXiv:1804.03599*, 2018.
- 566
- 567 Ricky TQ Chen, Xuechen Li, Roger B Grosse, and David K Duvenaud. Isolating sources of
568 disentanglement in variational autoencoders. *Advances in neural information processing systems*,
569 31, 2018.
- 570
- 571 Maxime Chevalier-Boisvert, Bolun Dai, Mark Towers, Rodrigo de Lazcano, Lucas Willems, Salem
572 Lahlou, Suman Pal, Pablo Samuel Castro, and Jordan Terry. Minigrid & miniworld: Modular &
573 customizable reinforcement learning environments for goal-oriented tasks. *CoRR*, abs/2306.13831,
574 2023.
- 575
- 576 Caleb Chuck, Kevin Black, Aditya Arjun, Yuke Zhu, and Scott Niekum. Granger causal interaction
577 skill chains. *Transactions on Machine Learning Research*, 2024. ISSN 2835-8856. URL <https://openreview.net/forum?id=iA2KQyoun1>.
- 578
- 579 Caleb Chuck, Fan Feng, Carl Qi, Chang Shi, Siddhant Agarwal, Amy Zhang, and Scott Niekum. Null
580 counterfactual factor interactions for goal-conditioned reinforcement learning. In *The Thirteenth*
581 *International Conference on Learning Representations*, 2025.
- 582
- 583 Pierre Comon. Independent component analysis, a new concept? *Signal processing*, 36(3):287–314,
584 1994.
- 585
- 586 Thomas Degris, Olivier Sigaud, and Pierre-Henri Wuillemin. Learning the structure of factored
587 markov decision processes in reinforcement learning problems. In *Proceedings of the 23rd*
588 *international conference on Machine learning*, pp. 257–264, 2006.
- 589
- 590 Thomas G Dietterich. Hierarchical reinforcement learning with the maxq value function decomposi-
591 tion. *Journal of artificial intelligence research*, 13:227–303, 2000.
- 592
- 593 Carlos Diuk, Lihong Li, and Bethany R Leffler. The adaptive k-meteorologists problem and its
594 application to structure learning and feature selection in reinforcement learning. In *Proceedings of*
595 *the 26th Annual International Conference on Machine Learning*, pp. 249–256, 2009.
- 596
- 597 Mhairi Dunion, Trevor McInroe, Kevin Sebastian Luck, Josiah P. Hanna, and Stefano V Albrecht.
598 Temporal disentanglement of representations for improved generalisation in reinforcement learning.
599 In *The Eleventh International Conference on Learning Representations*, 2023. URL <https://openreview.net/forum?id=sPgP6aISLTD>.

- 594 Mhairi Dunion, Trevor McInroe, Kevin Sebastian Luck, Josiah Hanna, and Stefano Albrecht. Condi-
595 tional mutual information for disentangled representations in reinforcement learning. *Advances in*
596 *Neural Information Processing Systems*, 36, 2024.
- 597 Carles Gelada, Saurabh Kumar, Jacob Buckman, Ofir Nachum, and Marc G Bellemare. Deepmdp:
598 Learning continuous latent space models for representation learning. In *International Conference*
599 *on Machine Learning*, pp. 2170–2179. PMLR, 2019.
- 600 Carlos Guestrin, Relu Patrascu, and Dale Schuurmans. Algorithm-directed exploration for model-
601 based reinforcement learning in factored mdps. In *Proceedings of the Nineteenth International*
602 *Conference on Machine Learning*, pp. 235–242, 2002.
- 603 Carlos Guestrin, Daphne Koller, Ronald Parr, and Shobha Venkataraman. Efficient solution algorithms
604 for factored mdps. *Journal of Artificial Intelligence Research*, 19:399–468, 2003.
- 605 Michael Gutmann and Aapo Hyvärinen. Noise-contrastive estimation: A new estimation principle
606 for unnormalized statistical models. In Yee Whye Teh and Mike Titterton (eds.), *Proceedings*
607 *of the Thirteenth International Conference on Artificial Intelligence and Statistics*, volume 9 of
608 *Proceedings of Machine Learning Research*, pp. 297–304, Chia Laguna Resort, Sardinia, Italy,
609 13–15 May 2010. PMLR.
- 610 Danijar Hafner, Timothy Lillicrap, Ian Fischer, Ruben Villegas, David Ha, Honglak Lee, and James
611 Davidson. Learning latent dynamics for planning from pixels. In *International conference on*
612 *machine learning*, pp. 2555–2565. PMLR, 2019.
- 613 Danijar Hafner, Jurgis Pasukonis, Jimmy Ba, and Timothy Lillicrap. Mastering diverse control tasks
614 through world models. *Nature*, pp. 1–7, 2025.
- 615 Nicklas A Hansen, Hao Su, and Xiaolong Wang. Temporal difference learning for model predictive
616 control. In *International Conference on Machine Learning*, pp. 8387–8406. PMLR, 2022.
- 617 Jonathan Heek, Anselm Levskaya, Avital Oliver, Marvin Ritter, Bertrand Rondepierre, Andreas
618 Steiner, and Marc van Zee. Flax: A neural network library and ecosystem for JAX, 2024. URL
619 <http://github.com/google/flax>.
- 620 Dan Hendrycks and Kevin Gimpel. Gaussian error linear units (gelus). *arXiv preprint*
621 *arXiv:1606.08415*, 2016.
- 622 Irina Higgins, Loic Matthey, Arka Pal, Christopher Burgess, Xavier Glorot, Matthew Botvinick,
623 Shakir Mohamed, and Alexander Lerchner. beta-VAE: Learning basic visual concepts with a
624 constrained variational framework. In *International Conference on Learning Representations*,
625 2017a.
- 626 Irina Higgins, Arka Pal, Andrei Rusu, Loic Matthey, Christopher Burgess, Alexander Pritzel, Matthew
627 Botvinick, Charles Blundell, and Alexander Lerchner. Darla: Improving zero-shot transfer in
628 reinforcement learning. In *International Conference on Machine Learning*, pp. 1480–1490. PMLR,
629 2017b.
- 630 Kyle Hsu, William Dorrell, James Whittington, Jiajun Wu, and Chelsea Finn. Disentanglement via
631 latent quantization. *Advances in Neural Information Processing Systems*, 36, 2024a.
- 632 Kyle Hsu, Jubayer Ibn Hamid, Kaylee Burns, Chelsea Finn, and Jiajun Wu. Tripod: Three comple-
633 mentary inductive biases for disentangled representation learning. In *International Conference on*
634 *Machine Learning*, pp. 19101–19122. PMLR, 2024b.
- 641 Jiaheng Hu, Zizhao Wang, Peter Stone, and Roberto Martín-Martín. Disentangled unsupervised
642 skill discovery for efficient hierarchical reinforcement learning. *Advances in Neural Information*
643 *Processing Systems*, 37:76529–76552, 2024.
- 644 Aapo Hyvärinen and Hiroshi Morioka. Unsupervised feature extraction by time-contrastive learning
645 and nonlinear ica. *Advances in neural information processing systems*, 29, 2016.
- 646 Aapo Hyvärinen, Ilyes Khemakhem, and Hiroshi Morioka. Nonlinear independent component
647 analysis for principled disentanglement in unsupervised deep learning. *Patterns*, 4(10), 2023.

- 648 Aapo Hyvärinen, Hiroaki Sasaki, and Richard Turner. Nonlinear ica using auxiliary variables and
649 generalized contrastive learning. In *The 22nd International Conference on Artificial Intelligence*
650 *and Statistics*, pp. 859–868. PMLR, 2019.
- 651
- 652 Nan Rosemary Ke, Aniket Rajiv Didolkar, Sarthak Mittal, Anirudh Goyal, Guillaume Lajoie, Stefan
653 Bauer, Danilo Jimenez Rezende, Yoshua Bengio, Christopher Pal, and Michael Curtis Mozer.
654 Systematic evaluation of causal discovery in visual model based reinforcement learning. In
655 *Thirty-fifth Conference on Neural Information Processing Systems Datasets and Benchmarks Track*
656 *(Round 2)*.
- 657 Michael Kearns and Daphne Koller. Efficient reinforcement learning in factored mdps. In *Proceedings*
658 *of the 16th international joint conference on Artificial intelligence-Volume 2*, pp. 740–747, 1999.
- 659
- 660 Michael Kearns and Satinder Singh. Near-optimal reinforcement learning in polynomial time.
661 *Machine learning*, 49:209–232, 2002.
- 662 Ilyes Khemakhem, Diederik Kingma, Ricardo Monti, and Aapo Hyvärinen. Variational autoencoders
663 and nonlinear ica: A unifying framework. In *International Conference on Artificial Intelligence*
664 *and Statistics*, pp. 2207–2217. PMLR, 2020a.
- 665
- 666 Ilyes Khemakhem, Ricardo Monti, Diederik Kingma, and Aapo Hyvärinen. Ice-beem: Identifiable
667 conditional energy-based deep models based on nonlinear ica. *Advances in Neural Information*
668 *Processing Systems*, 33:12768–12778, 2020b.
- 669 Hyunjik Kim and Andriy Mnih. Disentangling by factorising. In *International conference on machine*
670 *learning*, pp. 2649–2658. PMLR, 2018.
- 671
- 672 Diederik P. Kingma and Max Welling. Auto-encoding variational bayes. In Yoshua Bengio and Yann
673 LeCun (eds.), *2nd International Conference on Learning Representations, ICLR 2014, Banff, AB,*
674 *Canada, April 14-16, 2014, Conference Track Proceedings*, 2014.
- 675 David A Klindt, Lukas Schott, Yash Sharma, Ivan Ustyuzhaninov, Wieland Brendel, Matthias Bethge,
676 and Dylan Paiton. Towards nonlinear disentanglement in natural data with temporal sparse coding.
677 In *International Conference on Learning Representations*, 2020.
- 678
- 679 Daphne Koller and Ronald Parr. Policy iteration for factored mdps. In *Proceedings of the Sixteenth*
680 *conference on Uncertainty in artificial intelligence*, pp. 326–334, 2000.
- 681
- 682 Harold W Kuhn. The hungarian method for the assignment problem. *Naval research logistics*
683 *quarterly*, 2(1-2):83–97, 1955.
- 684 Sébastien Lachapelle, Pau Rodriguez, Yash Sharma, Katie E Everett, Rémi Le Priol, Alexandre
685 Lacoste, and Simon Lacoste-Julien. Disentanglement via mechanism sparsity regularization: A
686 new principle for nonlinear ica. In *Conference on Causal Learning and Reasoning*, pp. 428–484.
687 PMLR, 2022.
- 688
- 689 Sébastien Lachapelle, Pau Rodríguez López, Yash Sharma, Katie Everett, Rémi Le Priol, Alexandre
690 Lacoste, and Simon Lacoste-Julien. Nonparametric partial disentanglement via mechanism sparsity:
691 Sparse actions, interventions and sparse temporal dependencies. *arXiv preprint arXiv:2401.04890*,
692 2024.
- 693 Alex Lamb, Riashat Islam, Yonathan Efroni, Aniket Rajiv Didolkar, Dipendra Misra, Dylan J Foster,
694 Lekan P Molu, Rajan Chari, Akshay Krishnamurthy, and John Langford. Guaranteed discovery
695 of control-endogenous latent states with multi-step inverse models. *Transactions on Machine*
696 *Learning Research*, 2023.
- 697
- 698 Kuang-Huei Lee, Ian Fischer, Anthony Liu, Yijie Guo, Honglak Lee, John Canny, and Sergio
699 Guadarrama. Predictive information accelerates learning in rl. *Advances in Neural Information*
700 *Processing Systems*, 33:11890–11901, 2020.
- 701
- 701 Anson Lei, Bernhard Schölkopf, and Ingmar Posner. Variational causal dynamics: Discovering
modular world models from interventions. *arXiv preprint arXiv:2206.11131*, 2022.

- 702 Sergey Levine, Chelsea Finn, Trevor Darrell, and Pieter Abbeel. End-to-end training of deep
703 visuomotor policies. *Journal of Machine Learning Research*, 17(39):1–40, 2016. URL [http://](http://jmlr.org/papers/v17/15-522.html)
704 jmlr.org/papers/v17/15-522.html.
705
- 706 Timothy P Lillicrap, Jonathan J Hunt, Alexander Pritzel, Nicolas Heess, Tom Erez, Yuval Tassa,
707 David Silver, and Daan Wierstra. Continuous control with deep reinforcement learning. *4th*
708 *International Conference on Learning Representations*, 2016.
- 709 Phillip Lippe, Sara Magliacane, Sindy Löwe, Yuki M Asano, Taco Cohen, and Stratis Gavves. Citris:
710 Causal identifiability from temporal intervened sequences. In *International Conference on Machine*
711 *Learning*, pp. 13557–13603. PMLR, 2022.
712
- 713 Phillip Lippe, Sara Magliacane, Sindy Löwe, Yuki M Asano, Taco Cohen, and Efstratios Gavves.
714 Biscuit: Causal representation learning from binary interactions. In *Uncertainty in Artificial*
715 *Intelligence*, pp. 1263–1273. PMLR, 2023a.
- 716 Phillip Lippe, Sara Magliacane, Sindy Löwe, Yuki M Asano, Taco Cohen, and Efstratios Gavves.
717 Causal representation learning for instantaneous and temporal effects in interactive systems. In
718 *The Eleventh International Conference on Learning Representations*, 2023b.
719
- 720 Yuren Liu, Biwei Huang, Zhengmao Zhu, Honglong Tian, Mingming Gong, Yang Yu, and Kun
721 Zhang. Learning world models with identifiable factorization. *Advances in Neural Information*
722 *Processing Systems*, 36:31831–31864, 2023.
- 723 Francesco Locatello, Stefan Bauer, Mario Lucic, Gunnar Raetsch, Sylvain Gelly, Bernhard Schölkopf,
724 and Olivier Bachem. Challenging common assumptions in the unsupervised learning of disentangled
725 representations. In *international conference on machine learning*, pp. 4114–4124. PMLR,
726 2019.
727
- 728 Francesco Locatello, Ben Poole, Gunnar Rätsch, Bernhard Schölkopf, Olivier Bachem, and Michael
729 Tschannen. Weakly-supervised disentanglement without compromises. In *International conference*
730 *on machine learning*, pp. 6348–6359. PMLR, 2020.
- 731 Ilya Loshchilov and Frank Hutter. Decoupled weight decay regularization. In *International Confer-*
732 *ence on Learning Representations*, 2019. URL [https://openreview.net/forum?id=](https://openreview.net/forum?id=Bkg6RiCqY7)
733 [Bkg6RiCqY7](https://openreview.net/forum?id=Bkg6RiCqY7).
734
- 735 Dipendra Misra, Qinghua Liu, Chi Jin, and John Langford. Provable rich observation reinforcement
736 learning with combinatorial latent states. In *International Conference on Learning Representations*,
737 2021.
- 738 Volodymyr Mnih, Koray Kavukcuoglu, David Silver, Andrei A Rusu, Joel Veness, Marc G Bellemare,
739 Alex Graves, Martin Riedmiller, Andreas K Fidjeland, Georg Ostrovski, et al. Human-level control
740 through deep reinforcement learning. *nature*, 518(7540):529–533, 2015.
741
- 742 Tung D Nguyen, Rui Shu, Tuan Pham, Hung Bui, and Stefano Ermon. Temporal predictive coding
743 for model-based planning in latent space. In *International Conference on Machine Learning*, pp.
744 8130–8139. PMLR, 2021.
- 745 Aaron van den Oord, Yazhe Li, and Oriol Vinyals. Representation learning with contrastive predictive
746 coding. *arXiv preprint arXiv:1807.03748*, 2018.
747
- 748 Joseph Ortiz, Antoine Dedieu, Wolfgang Lehrach, J Swaroop Guntupalli, Carter Wendelken, Ahmad
749 Humayun, Sivaramkrishnan Swaminathan, Guangyao Zhou, Miguel Lázaro-Gredilla, and Kevin P
750 Murphy. Dmc-vb: A benchmark for representation learning for control with visual distractors.
751 *Advances in Neural Information Processing Systems*, 37:6574–6602, 2024.
- 752 Ian Osband and Benjamin Van Roy. Near-optimal reinforcement learning in factored mdps. *Advances*
753 *in Neural Information Processing Systems*, 27, 2014.
754
- 755 Eduardo Pignatelli, Jarek Liesen, Robert Tjarko Lange, Chris Lu, Pablo Samuel Castro, and Laura
Toni. Navix: Scaling minigrid environments with jax. *arXiv preprint arXiv:2407.19396*, 2024.

- 756 Silviu Pitis, Elliot Creager, and Animesh Garg. Counterfactual data augmentation using locally
757 factored dynamics. *Advances in Neural Information Processing Systems*, 33:3976–3990, 2020.
758
- 759 Silviu Pitis, Elliot Creager, Ajay Mandlekar, and Animesh Garg. Mocoda: Model-based counterfac-
760 tual data augmentation. *Advances in Neural Information Processing Systems*, 35:18143–18156,
761 2022.
- 762 Martin L. Puterman. *Markov Decision Processes: Discrete Stochastic Dynamic Programming*.
763 Wiley Series in Probability and Statistics. Wiley, 1994. ISBN 978-0-47161977-2. doi: 10.1002/
764 9780470316887.
- 765
- 766 Rafael Rodriguez-Sanchez and George Konidaris. Learning abstract world models for value-
767 preserving planning with options. *Reinforcement Learning Journal*, 4:1733–1758, 2024.
- 768
- 769 Max Rudolph, Caleb Chuck, Kevin Black, Misha Lvovsky, Scott Niekum, and Amy Zhang. Learning
770 action-based representations using invariance. *arXiv preprint arXiv:2403.16369*, 2024.
- 771 Jürgen Schmidhuber. Learning factorial codes by predictability minimization. *Neural computation*, 4
772 (6):863–879, 1992.
- 773
- 774 Bernhard Schölkopf, Francesco Locatello, Stefan Bauer, Nan Rosemary Ke, Nal Kalchbrenner,
775 Anirudh Goyal, and Yoshua Bengio. Toward causal representation learning. *Proceedings of the*
776 *IEEE*, 109(5):612–634, 2021.
- 777 Julian Schrittwieser, Ioannis Antonoglou, Thomas Hubert, Karen Simonyan, Laurent Sifre, Simon
778 Schmitt, Arthur Guez, Edward Lockhart, Demis Hassabis, Thore Graepel, et al. Mastering atari,
779 go, chess and shogi by planning with a learned model. *Nature*, 588(7839):604–609, 2020.
- 780
- 781 Maximilian Seitzer, Bernhard Schölkopf, and Georg Martius. Causal influence detection for improv-
782 ing efficiency in reinforcement learning. *Advances in Neural Information Processing Systems*, 34:
783 22905–22918, 2021.
- 784
- 785 Chandler Squires, Anna Seigal, Salil S Bhate, and Caroline Uhler. Linear causal disentanglement via
786 interventions. In *International conference on machine learning*, pp. 32540–32560. PMLR, 2023.
- 787
- 788 Alexander L. Strehl, Carlos Diuk, and Michael L. Littman. Efficient structure learning in factored-
789 state mdps. In *Proceedings of the 22nd National Conference on Artificial Intelligence - Volume 1*,
AAAI’07, pp. 645–650. AAAI Press, 2007. ISBN 9781577353232.
- 790
- 791 Richard S Sutton, Doina Precup, and Satinder Singh. Between mdps and semi-mdps: A framework
792 for temporal abstraction in reinforcement learning. *Artificial intelligence*, 112(1-2):181–211, 1999.
- 793
- 794 Valentin Thomas, Emmanuel Bengio, William Fedus, Jules Pondard, Philippe Beaudoin, Hugo
795 Larochelle, Joelle Pineau, Doina Precup, and Yoshua Bengio. Disentangling the independently
796 controllable factors of variation by interacting with the world. *arXiv preprint arXiv:1802.09484*,
2018.
- 797
- 798 Yi Tian, Jian Qian, and Suvrit Sra. Towards minimax optimal reinforcement learning in factored
799 markov decision processes. *Advances in Neural Information Processing Systems*, 33:19896–19907,
2020.
- 800
- 801 Burak Varici, Emre Acartürk, Karthikeyan Shanmugam, and Ali Tajer. General identifiability
802 and achievability for causal representation learning. In *International Conference on Artificial*
803 *Intelligence and Statistics*, pp. 2314–2322. PMLR, 2024.
- 804
- 805 Christopher M Vigorito and Andrew G Barto. Incremental structure learning in factored mdps with
806 continuous states and actions. *University of Massachusetts Amherst-Department of Computer*
807 *Science, Tech. Rep*, 2009.
- 808
- 809 Christopher M. Vigorito and Andrew G. Barto. Intrinsically motivated hierarchical skill learning in
structured environments. *IEEE Transactions on Autonomous Mental Development*, 2(2):132–143,
2010. doi: 10.1109/TAMD.2010.2050205.

- 810 Julius von Kügelgen, Michel Besserve, Liang Wendong, Luigi Gresele, Armin Kekić, Elias Barein-
811 boim, David Blei, and Bernhard Schölkopf. Nonparametric identifiability of causal representations
812 from unknown interventions. *Advances in Neural Information Processing Systems*, 36, 2024.
813
- 814 Tongzhou Wang, Simon S Du, Antonio Torralba, Phillip Isola, Amy Zhang, and Yuandong Tian. De-
815 noised mdps: Learning world models better than the world itself. *arXiv preprint arXiv:2206.15477*,
816 2022a.
- 817 Zizhao Wang, Xuesu Xiao, Zifan Xu, Yuke Zhu, and Peter Stone. Causal dynamics learning for
818 task-independent state abstraction. In Kamalika Chaudhuri, Stefanie Jegelka, Le Song, Csaba
819 Szepesvari, Gang Niu, and Sivan Sabato (eds.), *Proceedings of the 39th International Conference*
820 *on Machine Learning*, volume 162 of *Proceedings of Machine Learning Research*, pp. 23151–
821 23180, 17–23 Jul 2022b.
- 822 Zizhao Wang, Jiaheng Hu, Peter Stone, and Roberto Martín-Martín. Elden: Exploration via local
823 dependencies. *Advances in Neural Information Processing Systems*, 36:15456–15474, 2023.
824
- 825 Zizhao Wang, Jiaheng Hu, Caleb Chuck, Stephen Chen, Roberto Martín-Martín, Amy Zhang, Scott
826 Niekum, and Peter Stone. Skild: Unsupervised skill discovery guided by factor interactions.
827 In Amir Globersons, Lester Mackey, Danielle Belgrave, Angela Fan, Ulrich Paquet, Jakub M.
828 Tomczak, and Cheng Zhang (eds.), *Advances in Neural Information Processing Systems 38:*
829 *Annual Conference on Neural Information Processing Systems 2024, NeurIPS 2024, Vancouver,*
830 *BC, Canada, December 10 - 15, 2024*, 2024.
- 831 Ziping Xu and Ambuj Tewari. Near-optimal reinforcement learning in factored mdps: Oracle-efficient
832 algorithms for the non-episodic setting. *Advances in Neural Information Processing Systems*, 33,
833 2020.
- 834 Qi Yi, Rui Zhang, Shaohui Peng, Jiaming Guo, Xing Hu, Zidong Du, Qi Guo, Ruizhi Chen, Ling
835 Li, and Yunji Chen. Learning controllable elements oriented representations for reinforcement
836 learning. *Neurocomputing*, 549:126455, 2023.
837
- 838 Amy Zhang, Rowan Thomas McAllister, Roberto Calandra, Yarín Gal, and Sergey Levine. Learning
839 invariant representations for reinforcement learning without reconstruction. In *International*
840 *Conference on Learning Representations*, 2021. URL [https://openreview.net/forum?](https://openreview.net/forum?id=-2FCwDKRREu)
841 [id=-2FCwDKRREu](https://openreview.net/forum?id=-2FCwDKRREu).
- 842 Jiaqi Zhang, Kristjan Greenewald, Chandler Squires, Akash Srivastava, Karthikeyan Shanmugam,
843 and Caroline Uhler. Identifiability guarantees for causal disentanglement from soft interventions.
844 *Advances in Neural Information Processing Systems*, 36:50254–50292, 2023.
845
846
847
848
849
850
851
852
853
854
855
856
857
858
859
860
861
862
863

A THEORETICAL RESULTS

Definition A.1 (Identifiability). An encoder $f : X \rightarrow Z$ identifies \mathcal{S} if there exists a permutation π and functions $h_i : \mathcal{S}_i \rightarrow Z_{\pi(i)}$ that are diffeomorphism such that $s_i = h(z_{\pi(i)})$. That is, each latent factor learned is equivalent to a ground truth factor up to a permutation.

Lemma A.2 (Local Identifiability of the Independently Controllable Factors). *Let the learned encoder $f : X \rightarrow Z$ be a diffeomorphism. If the following conditions hold*

1. *The action effects are **sufficiently different** from the natural dynamics. That is, there exists $i \in [K]$*

$$\frac{\partial}{\partial s'_i} T_i(s'_i | s, a) \neq 0$$

for $s \in \tilde{S} \subseteq \mathcal{S}$, almost surely. Moreover, there exists at least an action that affects each s_i (independently controllability)

2. *All energy function approximate the factor forward dynamics $E(z'_i, a, z) \propto \log T(z'_i | z, a)$;*
3. (**Sparsity**) *The learned score differences*

$$\frac{\partial}{\partial z'_i} \Delta E_i^a = \frac{\partial}{\partial z'_i} [E(z'_i, a, z) - E(z'_i, a_0, z)] \neq 0$$

for at most one variable j .

then, there exists a factor-wise diffeomorphism $h : \mathcal{S} \rightarrow Z$ between the learned encoding Z and the underlying ground truth factors of variation \mathcal{S} .

Proof. Let h be a diffeomorphism between \mathcal{S} and Z . Given that the ground truth observation function is a diffeomorphism $o : \mathcal{S} \rightarrow X$ and, by assumption, the learned encoding is also a diffeomorphism. We can see that $h(s) = f(o(s))$. We need to prove that there exists a permutation $\pi : [K] \rightarrow [K]$ such that the permuted Jacobian of h , $P_\pi J_h$, is a diagonal matrix.

Given that h is a diffeomorphism, J_h exists.

Moreover, for each binary classifier, we know that at an optimum they converge to:

$$\log \frac{T(s' | s, a_n)}{T(s' | s, a_0)} = \sum_{l=1}^K E(z'_l, a_n, z) - E(z'_l, a_0, z) + C(z, a_n) \quad \forall a_n \in A \setminus \{a_0\}; \quad (7)$$

where $C(z, a)$ is a constant resulting from the normalization constants that are not estimated in ACF. By taking the gradient with respect to s' using the chain rule, we get that

$$\nabla_{s'} \log \frac{T(s' | s, a_n)}{T(s' | s, a_0)} = \sum_{l=1}^K J_h^T(s') \nabla_{z'} [E(z'_l, a_n, z) - E(z'_l, a_0, z)] \quad \forall a_n \in A \setminus \{a_0\} \quad (8)$$

Let $\rho(a_i) \mapsto [K]$ be the maps each action to its affected factor. Hence, by considering our sparse interaction model in Equation 1 we get that each classifier is a function of the variables affected by a_n . That is,

$$\begin{aligned} \nabla_{s'} \log \frac{T(s'_{\rho(a_n)} | s, a_n)}{T(s'_{\rho(a_n)} | s, a_0)} &= \sum_{l=1}^K J_h^T(s') \nabla_{z'} [E(z'_l, a_n, z) - E(z'_l, a_0, z)] \quad \forall a_n \in A \setminus \{a_0\} \quad (9) \\ &= J_h^T \begin{bmatrix} \frac{\partial}{\partial z'_1} (E(z'_1, a_n, z) - E(z'_1, a_0, z)) \\ \vdots \\ \frac{\partial}{\partial z'_K} (E(z'_K, a_n, z) - E(z'_K, a_0, z)) \end{bmatrix} \quad (10) \end{aligned}$$

Moreover, consider a set of the actions $\bar{\mathcal{A}} \subseteq \mathcal{A} \setminus \{a_0\}$ such that each action affects one of the ground truth variables, that is, they are independently controllable.

We can write the above conditions in matrix form by stacking the gradients of all the actions in $\bar{\mathcal{A}}$.

Let $\Delta S(z' | z)$ be the matrices of learned score differences

$$[\Delta S(z' | z)]_{l,n} = \frac{\partial}{\partial z'_l} [E(z'_l, a_n, z) - E(z'_l, a_0, z)]; \quad (11)$$

and $\Delta S(s' | s)$ be the matrices of score differences in s' .

$$[\Delta S(s' | s)]_{i,n} = \begin{cases} \frac{\partial}{\partial s'_i} \log \frac{T(s'_i | s, a_n)}{T(s'_i | s, a_0)} & \text{if } i = \rho(a_n) \\ 0 & \text{otherwise} \end{cases} \quad (12)$$

Hence, we can rewrite Equation 8 as

$$\Delta S(s' | s) = J_h^T(s') \Delta S(z' | z). \quad (13)$$

There exists s such that all columns of $\Delta S(s' | s)$ has only one element different from zero and it is full rank because each factor is affected by at least one action. Moreover, given $J_h(s')$ is full rank because is a diffeomorphism and $\Delta S(z' | z)$ must also have exactly one element different from zero (sparsity condition).

Thus, $J_h(s')$ must have only one element different from zero per row. To see this, consider the j th column of $\Delta S(z' | z)_j = \beta e_r$ where $\beta \in \mathbb{R}$ and r is the row different from zero. Hence,

$$\begin{aligned} \Delta S(s' | s)_j &= J_h^T(s') \Delta S(z' | z)_j; \\ &= \beta J_h^T(s') e_r; \\ &= \beta J_h^T(s')_{:,r}; \end{aligned}$$

and, therefore, $J_h(s')_r$ the r th column of the Jacobian must have one element different from zero. Therefore, $J_h(s')$ must be 1-sparse.

Finally, there exists a permutation $P(s')$ such that $J_h(s') = P(s')D(s')$ where $D(s')$ is a diagonal matrix. That is, there exists h that is a factorwise transformation of s up to a permutation.

□

This lemma shows that there exists a permutation in s where action can have independent control over the factors. However, this does not guarantee the encoding is consistent because the permutation could be different in other parts of the space.

The following proposition establishes some conditions that guarantee identifiability globally.

Proposition A.3 (Global Identifiability of Independently Controllable Factors). *Let the local conditions for identifiability hold. Moreover, assume that $S \subseteq \mathbb{R}^K$ is connected. Then there exists a unique permutation π for all $s \in S$.*

Proof. Let $s_0 \in S$ be a fix point. We know that the Jacobian $J_h(s_0) = P_{\pi}(s_0)D(s_0)$ because of local identifiability. Let π_{s_0} be the permutation corresponding to the matrix $P_{\pi}(s_0)$.

Moreover, because h is a diffeomorphism, we have that each derivative $h'_i(s)$ is continuous and non-vanishing.

Therefore, there exists a neighborhood U such that $h_{\pi_{s_0}(i)}(s_{\pi_{s_0}(i)}) \neq 0$ for all $s \in U$.

Because of continuity of J_h , we must have that per each row it's nonzero element remains so and, similarly, for the zero elements of the row. Therefore, the permutation $\pi_{s_0} = \pi_s$ for all $s \in U$. This makes the permutation locally constant.

Finally, because there’s a finite discrete number of permutations and \mathcal{S} is connected, it implies that $\pi_s = \pi$ globally constant in \mathcal{S} .

□

B EXTENDED EMPIRICAL RESULTS

Anonymized code at https://anonymous.4open.science/r/factored_rl-EE0A.

B.1 NETWORK ARCHITECTURES

All networks were implemented using JAX (Bradbury et al., 2018) and Flax NNX (Heek et al., 2024).

Table 2: All methods use the same Residual Convolutional architecture for encoder (and decoder, when required). All MLPs use SiLU activations. Latent encodings are Tanh to keep between $(-1, 1)$ except for DMS.

Component	DoorKey(8x8)	Taxi	Grid2D	FourRooms
latent_dim (d)	7	6	2	5
n_actions n_a	10	6	5	10
ACF Energy[$\times d$]	$(d + n_a) \rightarrow 256 \rightarrow n_a$			
ACF Inverse	$2d \rightarrow 128 \rightarrow n_a$			
ACF Policy	$d \rightarrow 256 \rightarrow 256 \rightarrow n_a$			
GCL Energy[$\times d$]	$(d + n_a) \rightarrow 128 \rightarrow 128 \rightarrow n_a$			
DMS Transition[$\times d$]	$(d + n_a) \rightarrow 256 \rightarrow 1$			
Markov Inverse	$2d \rightarrow 128 \rightarrow n_a$			
Markov Ratio	$2d \rightarrow 128 \rightarrow 1$			

Pixel-level Encoder & Decoder.

We parameterize the residual blocks by doubling the depth of the output feature map until reaching a minimum resolution (`min_res`) (4 for all our experiments) starting from a minimum depth (24 for all our experiments). This is similar to the residual CNN used in Hafner et al. (2025). Table 2 show the details of the MLPs used.

- **Residual Encoder:**
 - Positional Embeddings (x, y channels).
 - Cascade of downsampling ResidualBlocks: stride-2 3×3 convolution \rightarrow RMSNorm \rightarrow SiLU, plus two 1×1 conv residual layers.
 - Flatten \rightarrow 2-layer MLP ($256 \rightarrow 256$, SiLU, then Tanh) \rightarrow latent_dim(d)
- **Residual Decoder:**
 - MLP up-projection from latent_dim \rightarrow min_res \times min_res \times D .
 - Stack of transposed ResidualBlocks (stride-2 conv^T, RMSNorm, SiLU, ...)
 - Central crop to $32 \times 32 \rightarrow$ Tanh activation.
- **MLPs** All MLPs have SiLU activations (Hendrycks & Gimpel, 2016).

B.2 DOMAINS

In all domains we collected data by ensuring coverage of the state-action space. **Grid2D**

Actions No-op, Up, Down, Left, Right;

State Space Continuous 2D space

1026 **Observations** $32 \times 32 \times 3$ pixel rendering.

1027
1028 **Taxi implementation in JAX.**

1029
1030 **Actions** No-op, Up, Down, Left, Right;

1031 **State Space** 5×5 , 1 passenger, 4 different goals positions;

1032 **Observations** 32×32 RGB rendering.

1033
1034 **Minigrid-FourRooms & Minigrid-DoorKey(8x8)**

1035
1036 **Actions** No-op, Rotate clockwise, Rotate counterclockwise, Forward, Backward, Right, Left, Pickup,
1037 Open, Done;

1038 **State Space** 16×16 grid (position) and orientation (North, South, East, West);

1039 **Observation** RGB 32×32 rendering.

1040

1041 B.3 HYPERPARAMETERS, TUNING AND COMPUTATIONAL RESOURCES

1042

1043 We tune the hyperparameters by random search allocating 50 samples to each method and each
1044 configuration run with 5 different seeds. Tables 3, 4, 5, and 6 show the details for the best results for
1045 all methods and domains. Each trial was run in a NVIDIA GeForce RTX3090 24GB. Each trial took
1046 15min. All experiments used 150K transitions.

1047

1048 Table 3: Hyperparameters and coefficient weights for the ACF baseline across four domains.

1049

Hyperparameter	DoorKey-Uniform	Taxi	Grid2D	FourRooms
<i>Training</i>				
batch_size	128	128	128	128
lr	4.0966×10^{-4}	2.9126×10^{-4}	2.27497×10^{-4}	3.6392×10^{-4}
epochs	100	200	200	200
<i>ACF Coefficients</i>				
λ_{fwd}	97.815	31.444	95.395	40.736
λ_r	25.623	5.018	48.560	16.963
λ_{inv}	22.094	1.000	1.000	97.365
λ_π	1.610	9.916	1.332	22.764

1059

1060

1061 Table 4: Hyperparameters and coefficient weights for the GCL baseline across domains.

1062

Hyperparameter	DoorKey(8x8)	Taxi	Grid2D	FourRooms
<i>Training</i>				
batch_size	128	128	128	128
lr	2.0363×10^{-4}	4.4530×10^{-4}	1.6031×10^{-4}	2.7661×10^{-5}
epochs	100	200	200	200
<i>GCL Coefficients</i>				
classifier_coeff	60.444	27.293	90.737	51.030
recons_coeff	9.26×10^{-8}	4.53×10^{-10}	0.193	3.50×10^{-4}

1070

1071

1072

1073

1074

1075

1076

1077

1078

1079

B.4 DETAILED EMPIRICAL RESULTS

Detailed results for DoorKey (Figure ??), Minigrid-FourRooms (Figure 6), Taxi (Figure 7b), and Grid2D (Figure 8).

1080
 1081
 1082
 1083
 1084
 1085
 1086
 1087
 1088
 1089
 1090
 1091
 1092
 1093
 1094
 1095
 1096
 1097
 1098
 1099
 1100
 1101
 1102
 1103
 1104
 1105
 1106
 1107
 1108
 1109
 1110
 1111
 1112
 1113
 1114
 1115
 1116
 1117
 1118
 1119
 1120
 1121
 1122
 1123
 1124
 1125
 1126
 1127
 1128
 1129
 1130
 1131
 1132
 1133

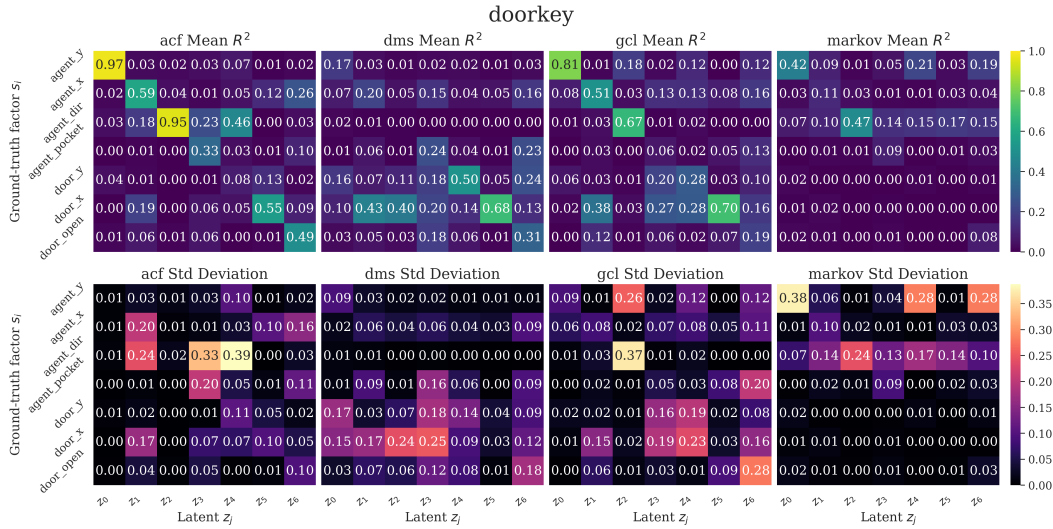
Table 5: Hyperparameters and coefficient weights for the DMS baseline across domains.

Hyperparameter / Coefficient	DoorKey(8x8)	Taxi	Grid2D	FourRooms
<i>Training</i>				
batch_size	128	128	128	128
lr	3.5332×10^{-4}	9.6832×10^{-5}	7.5007×10^{-5}	4.0218×10^{-4}
epochs	100	200	200	200
<i>DMS Coefficients</i>				
elbo_const	4.737	67.349	42.948	5.225
action_sparsity_const	3.536	36.881	91.982	9.878
state_sparsity_const	2.557	8.024	1.000	6.091
gumbel_temp	7.417	1.000	6.360	3.465
l2_reg_const	0.0015	0.0023	0.2805	0.0060

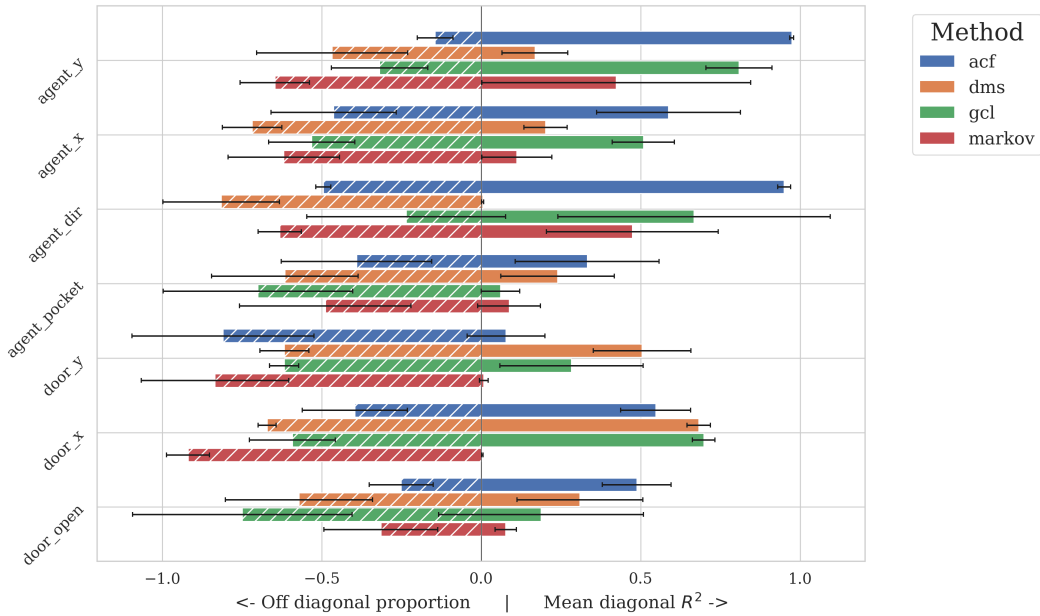
Table 6: Hyperparameters and coefficient weights for the Markov baseline across domains.

Hyperparameter / Coefficient	DoorKey(8x8)	Taxi	Grid2D	FourRooms
<i>Training</i>				
batch_size	128	128	128	128
lr	4.5536×10^{-4}	3.9622×10^{-4}	4.2654×10^{-4}	1.5854×10^{-4}
epochs	100	200	200	200
<i>Markov Coefficients</i>				
inverse_const	6.009	66.916	78.480	9.472
ratio_const	8.519	42.518	1.000	0.311
smoothness_const	2.092	8.234	84.905	9.691

1134
1135
1136
1137
1138
1139
1140
1141
1142
1143
1144
1145
1146
1147
1148
1149
1150
1151
1152
1153
1154
1155
1156
1157
1158
1159
1160
1161
1162
1163
1164
1165
1166
1167
1168
1169
1170
1171
1172
1173
1174
1175
1176
1177
1178
1179
1180
1181
1182
1183
1184
1185
1186
1187



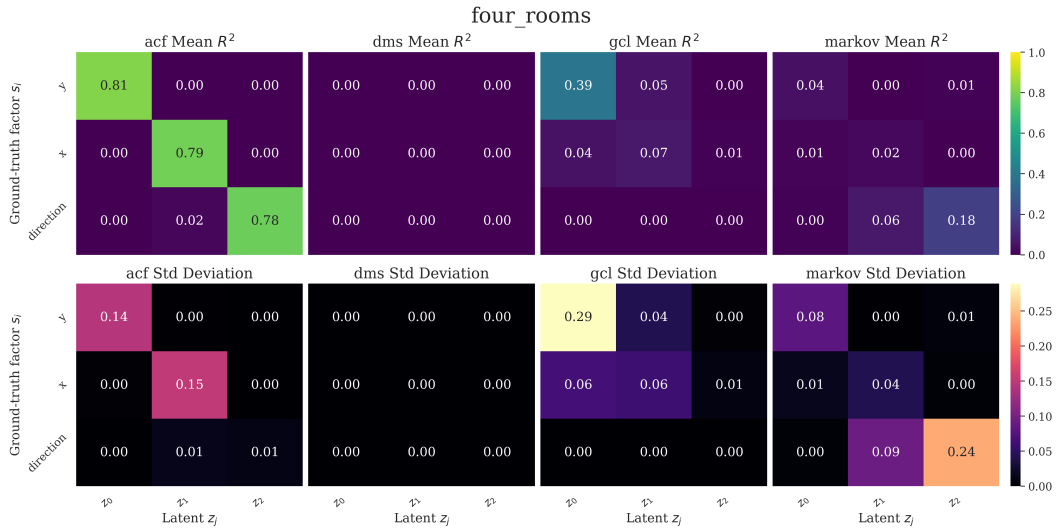
(a) R^2 matrices for **DoorKey** (8x8) for 5 seeds: [Top] Mean R^2 matrices. [Bottom] Standard Deviation



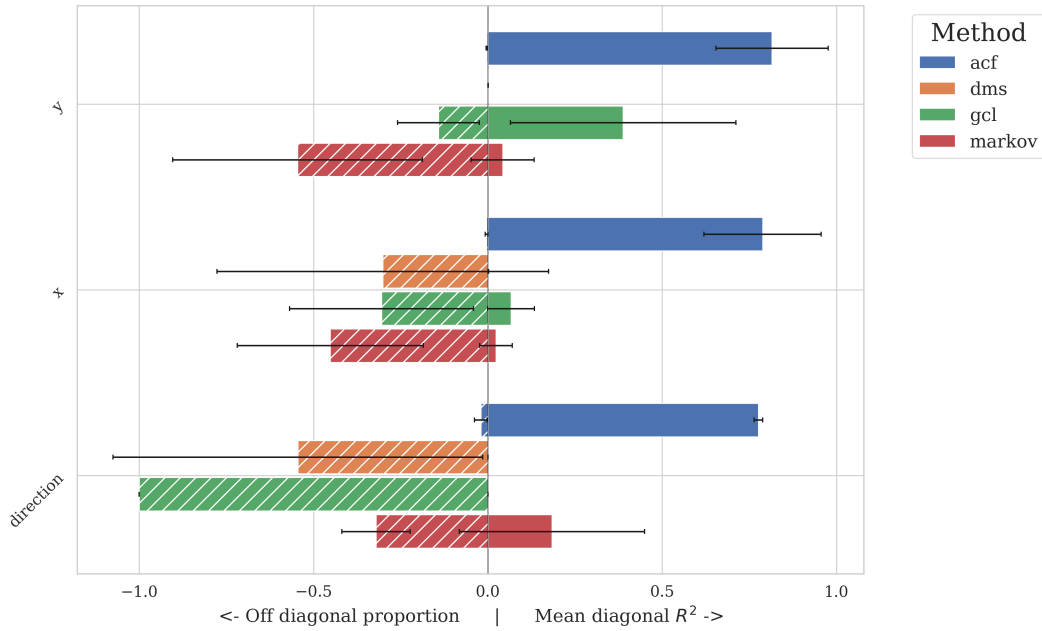
(b) Off diagonal proportion vs. Mean diagonal value per state

Figure 5: **DoorKey** Factorization Results

1188
1189
1190
1191
1192
1193
1194
1195
1196
1197
1198
1199
1200
1201
1202
1203
1204
1205
1206
1207
1208
1209
1210
1211
1212
1213
1214
1215
1216
1217
1218
1219
1220
1221
1222
1223
1224
1225
1226
1227
1228
1229
1230
1231
1232
1233
1234
1235
1236
1237
1238
1239
1240
1241

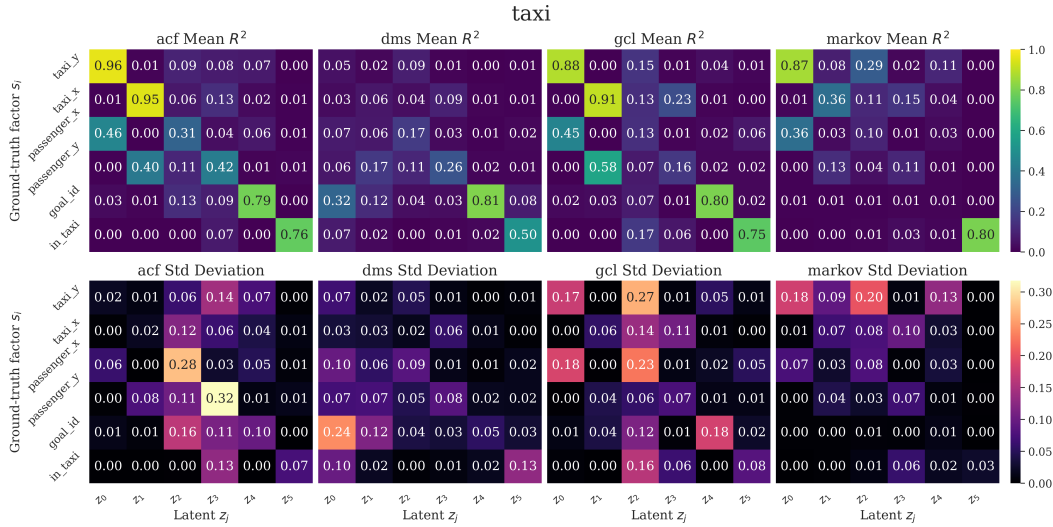


(a) R^2 matrices for Minigrid-FourRooms for 5 seeds: [Top] Mean R^2 matrices. [Bottom] Standard Deviation

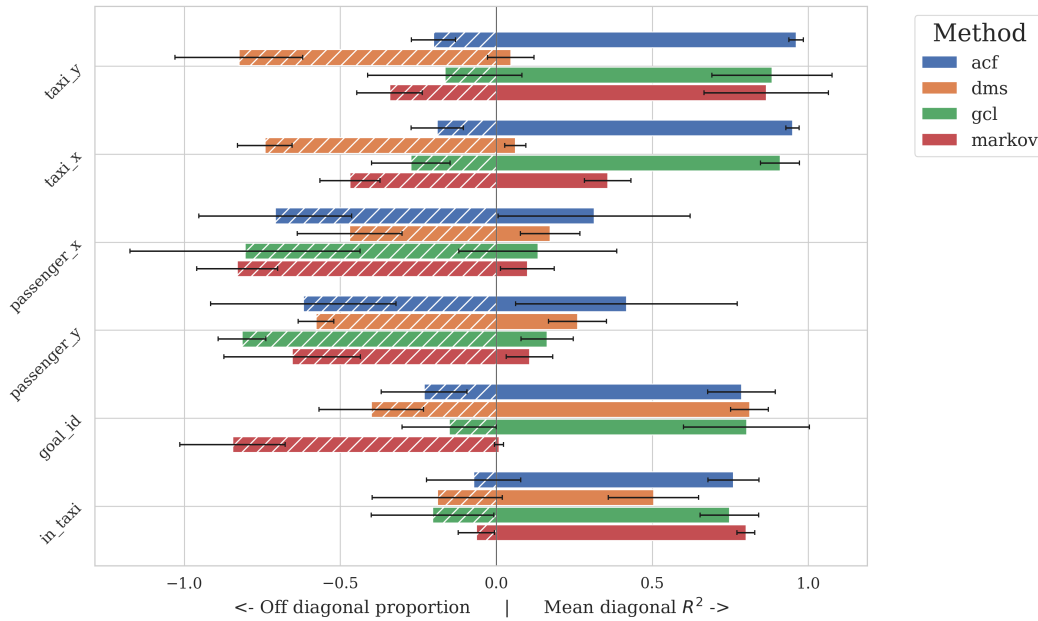


(b) Off diagonal proportion vs. Mean diagonal value per state

Figure 6: Minigrid-FourRooms Factorization Results



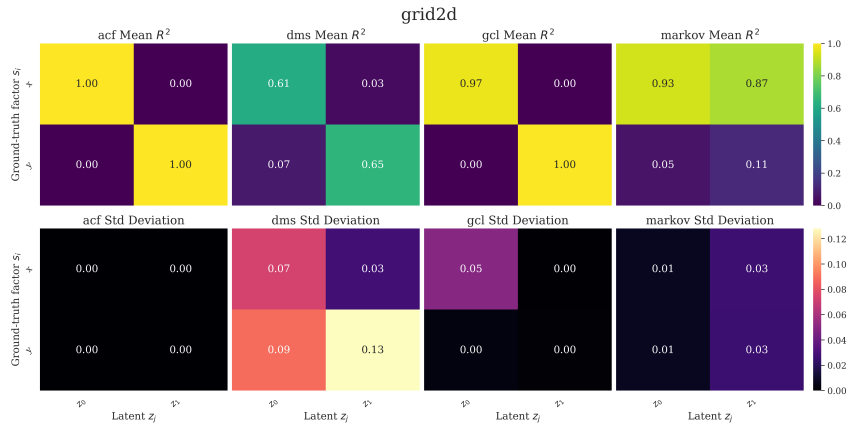
(a) R^2 matrices for **Taxi** for 5 seeds: [Top] Mean R^2 matrices. [Bottom] Standard Deviation



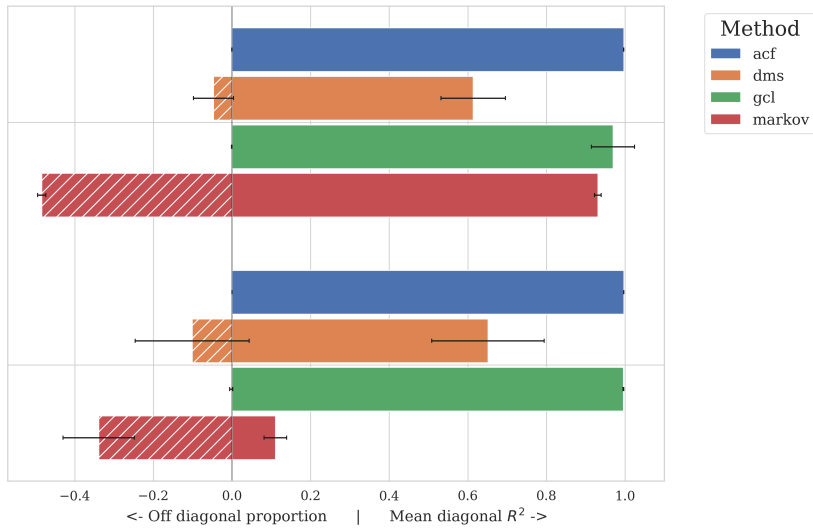
(b) Off diagonal proportion vs. Mean diagonal value per state

Figure 7: **Taxi** Factorization Results

1296
1297
1298
1299
1300
1301
1302
1303
1304
1305
1306
1307
1308
1309
1310
1311
1312
1313
1314
1315
1316
1317
1318
1319
1320
1321
1322
1323
1324
1325
1326
1327
1328
1329
1330
1331
1332
1333
1334
1335
1336
1337
1338
1339
1340
1341
1342
1343
1344
1345
1346
1347
1348
1349



(a) R^2 matrices for **Grid2D** for 5 seeds: [Top] Mean R^2 matrices. [Bottom] Standard Deviation



(b) Off diagonal proportion vs. Mean diagonal value per state

Figure 8: **Grid2D** Factorization Results